ORIGINAL ARTICLE

A Tracheal Aspirate-derived Airway Basal Cell Model Reveals a Proinflammatory Epithelial Defect in Congenital Diaphragmatic Hernia

Richard Wagner[1,2,3*], Gaurang M. Amonkar[1,2*], Wei Wang[1], Jessica E. Shui[1], Kamakshi Bankoti[1], Wai Hei Tse[4], Frances A. High[2,5,6], Jill M. Zalieckas[7], Terry L. Buchmiller[7], Augusto Zani[8], Richard Keijzer[4], Patricia K. Donahoe[2], Paul H. Lerou[1‡], and Xingbin Ai[1‡]

[1]Division of Newborn Medicine and [6]Division of Medical Genetics, Department of Pediatrics, and [2]Pediatric Surgical Research Laboratories, Department of Surgery, Massachusetts General Hospital, Harvard Medical School, Boston, Massachusetts; [3]Department of Pediatric Surgery, University Hospital Leipzig, Leipzig, Germany; [4]Departments of Surgery, Pediatrics & Child Health, Physiology & Pathophysiology, University of Manitoba and Children's Hospital Research Institute of Manitoba, Winnipeg, Manitoba, Canada; [5]Department of Surgery and [7]Division of Pediatric Surgery, Department of Surgery, Boston Children's Hospital, Harvard Medical School, Boston, Massachusetts; and [8]Department of Pediatric Surgery, University of Toronto, Hospital for Sick Children, Toronto, Ontario, Canada

ORCID IDs: 0000-0002-3035-2619 (R.W.); 0000-0002-7238-7131 (G.M.A.).

Abstract

Rationale: Congenital diaphragmatic hernia (CDH) is characterized by incomplete closure of the diaphragm and lung hypoplasia. The pathophysiology of lung defects in CDH is poorly understood.

Objectives: To establish a translational model of human airway epithelium in CDH for pathogenic investigation and therapeutic testing.

Methods: We developed a robust methodology of epithelial progenitor derivation from tracheal aspirates of newborns. Basal stem cells (BSCs) from patients with CDH and preterm and term non-CDH control subjects were derived and analyzed by bulk RNA sequencing, assay for transposase accessible chromatin with sequencing, and air–liquid interface differentiation. Lung sections from fetal human CDH samples and the nitrofen rat model of CDH were subjected to histological assessment of epithelial defects. Therapeutics to restore epithelial differentiation were evaluated in human epithelial cell culture and the nitrofen rat model of CDH.

Measurements and Main Results: Transcriptomic and epigenetic profiling of CDH and control BSCs reveals a proinflammatory signature that is manifested by hyperactive nuclear factor kappa B and independent of severity and hernia size. In addition, CDH BSCs exhibit defective epithelial differentiation *in vitro* that recapitulates epithelial phenotypes found in fetal human CDH lung samples and fetal tracheas of the nitrofen rat model of CDH. Furthermore, blockade of nuclear factor kappa B hyperactivity normalizes epithelial differentiation phenotypes of human CDH BSCs *in vitro* and in nitrofen rat tracheas *in vivo*.

Conclusions: Our findings have identified an underlying proinflammatory signature and BSC differentiation defects as a potential therapeutic target for airway epithelial defects in CDH.

Keywords: congenital diaphragmatic hernia; lung hypoplasia; tracheal aspirate derived lung progenitor cells; inflammatory gene expression signature; nitrofen rat model

(Received in original form May 19, 2022; accepted in final form February 2, 2023)

*These authors contributed equally to this work.

‡Senior author.

Supported by a grant from the German Research Foundation (DFG) (461188606 [R.W.]); the NIH (NICHD 2PO1HD068250 [P.K.D.] and R21AI156597 [P.H.L.]); and funds from the Department of Pediatrics at MGH for the Lung Cell Bank (X.A.).

Author Contributions: R.W., G.M.A., P.K.D., P.H.L., and X.A. conceived the study. R.W., G.M.A., W.W., K.B., J.E.S., W.H.T., and X.A. performed experiments. W.W., R.W., and X.A. analyzed bioinformatic data. P.K.D., F.A.H., P.H.L., and X.A. coordinated the study. R.K., J.M.Z., T.L.B., and A.Z. provided crucial samples. R.W., G.M.A., and X.A. wrote the manuscript. All authors critically read the manuscript.

Correspondence and requests for reprints should be addressed to Xingbin Ai, Ph.D., Division of Newborn Medicine, Department of Pediatrics, Massachusetts General Hospital, Harvard Medical School, 55 Fruit St, Boston, MA 02114. E-mail: xai@mgh.harvard.edu.

This article has a related editorial.

This article has an online supplement, which is accessible from this issue's table of contents at www.atsjournals.org.

Am J Respir Crit Care Med Vol 207, Iss 9, pp 1214–1226, May 1, 2023

Originally Published in Press as DOI: 10.1164/rccm.202205-0953OC on February 2, 2023
Internet address: www.atsjournals.org

At a Glance Commentary

Scientific Knowledge on the Subject: Congenital diaphragmatic hernia is characterized by lung hypoplasia, pulmonary hypertension, and a diaphragmatic defect. Because of a lack of translational models, the underlying pathobiology is poorly understood.

What This Study Adds to the Field: We provide a new *in vitro* model to study human congenital diaphragmatic hernia lung phenotypes via tracheal aspirate-derived airway basal cells. Using this model, we identified the hyperactivation of nuclear factor kappa B as a potential therapeutic target to normalize epithelial phenotypes in congenital diaphragmatic hernia.

Congenital diaphragmatic hernia (CDH) affects 1 out of 3,000 live births and is characterized by abnormal development of the lung and diaphragm (1–4). Lung hypoplasia in CDH features reduced airway branching, impaired alveolarization, and thickened mesenchyme. Surgical repair of the diaphragm and current nonsurgical treatments still cannot fully prevent significant mortality and long-term complications in survivors (5, 6).

The etiology of lung defects in CDH is complex. In addition to mechanical compression as a contributing factor (7–9), pathogenic mechanisms inherent to lung development also underlie lung hypoplasia in CDH (3, 10, 11). For example, a few CDH-associated genes play primary roles in the formation of airway epithelium and lung mesenchyme (12–16). In an established CDH model induced by oral nitrofen administration to pregnant rat dams (17), lung abnormalities in exposed fetuses are evident before the closure of the diaphragm (3). Despite these findings in animal models, pathogenic changes in the human CDH lung remain poorly characterized because of limited access to neonatal lung tissue. Lung biopsy at the time of surgery is contraindicated, and postmortem lung tissues are rare and often affected by artifacts from clinical procedures and tissue handling (18). To directly study lung defects in human CDH, translational models of patient-specific epithelium and mesenchyme are needed.

Basal stem cells (BSCs) are multipotent progenitor cells localized along the entire conducting airways in humans, whereas they are restricted to the trachea and main bronchi in rodents (19–21). BSCs can self-renew and give rise to multiple epithelial cell types during development, homeostasis, and regeneration after injury (19, 22, 23). Importantly during the early stages of lung development, $TP63^{+}$ lineage-labeled epithelial progenitors can generate both proximal and distal epithelium (24). A useful *in vitro* model of functional airway epithelium is air–liquid interface (ALI) culture in which BSCs differentiate into multiple epithelial cell types (25).

Tracheal aspirates (TAs) can be collected during routine care of intubated patients and are considered medical waste. TAs contain epithelial and mesenchymal progenitors and provide a renewable surrogate of neonatal lung tissue (26–29).

To investigate epithelial defects in patients with CDH, we derived BSCs from TAs of newborns with CDH and preterm, term, and non-CDH control subjects. Using multimodal analyses of BSCs and histological characterization of lung samples from human CDH fetuses and the nitrofen rat CDH model, we have identified a proinflammatory signature of CDH BSCs that causes differentiation defects of the airway epithelium in CDH.

Some of the results of these studies have been previously reported in the form of a preprint (bioRxiv, 12 Nov 2022, www.biorxiv.org/content/10.1101/2022.11.10.515365v1).

Table 1. Demographic and Clinical Information of Patients with Congenital Diaphragmatic Hernia from Whom Tracheal Aspirate Basal Stem Cells Were Derived and the Summary of Assays Performed for Each Congenital Diaphragmatic Hernia Basal Stem Cell Line

Patient #	Sex	Gestational Age (wk)	Survival (Y/N)	Side	Defect Size	ECMO (Y/N)	Comorbidities	Differentiated (Y/N)	Assay
1	M	38	Y	L	C type	N	Mild coarctation	Y	RS, A, D
2	M	39	Y	L	C type	Y	Isolated	Y	RS, A, D
3	M	39	Y	R	A type	N	VAWH, BAV	N	RS, D
4	M	28	Y	R	B type	N	Bilateral grade II IVH with cystic changes	N	RS, D
5	M	39	Y	L	B type	N	Isolated	Y	RS, D
6	M	37	Y	L	C type	Y	Isolated	Y	RS, D
7	M	36	Y	L	C type	Y	Hypospadia, cryptorchidism, camptodactyly, IUGR	N	RS, D
8	F	37	Y	L	C type	N	Isolated	Y	RS, D
9	M	37	Y	L	C type	Y	Isolated	N	RS, D
10	M	39	Y	L	C type	Y	Isolated	Y	RS, D
11	M	39	Y	L	D type	Y	Isolated	Y	RS, D
12	M	37	Y	R	D type	Y	Isolated	N	RS, D
13	M	38	Y	R	B type	Y	Tetralogy of fallot	N	D

Definition of abbreviations: A = assay for transposase accessible chromatin with sequencing; BAV = bicuspid aortic valve; D = differentiation; ECMO = extracorporeal membrane oxygenation; IUGR = intrauterine growth restriction; IVH = intraventricular hemorrhage; L = left; R = right; RS = RNA sequencing; VAWH = ventral abdominal wall hernia.

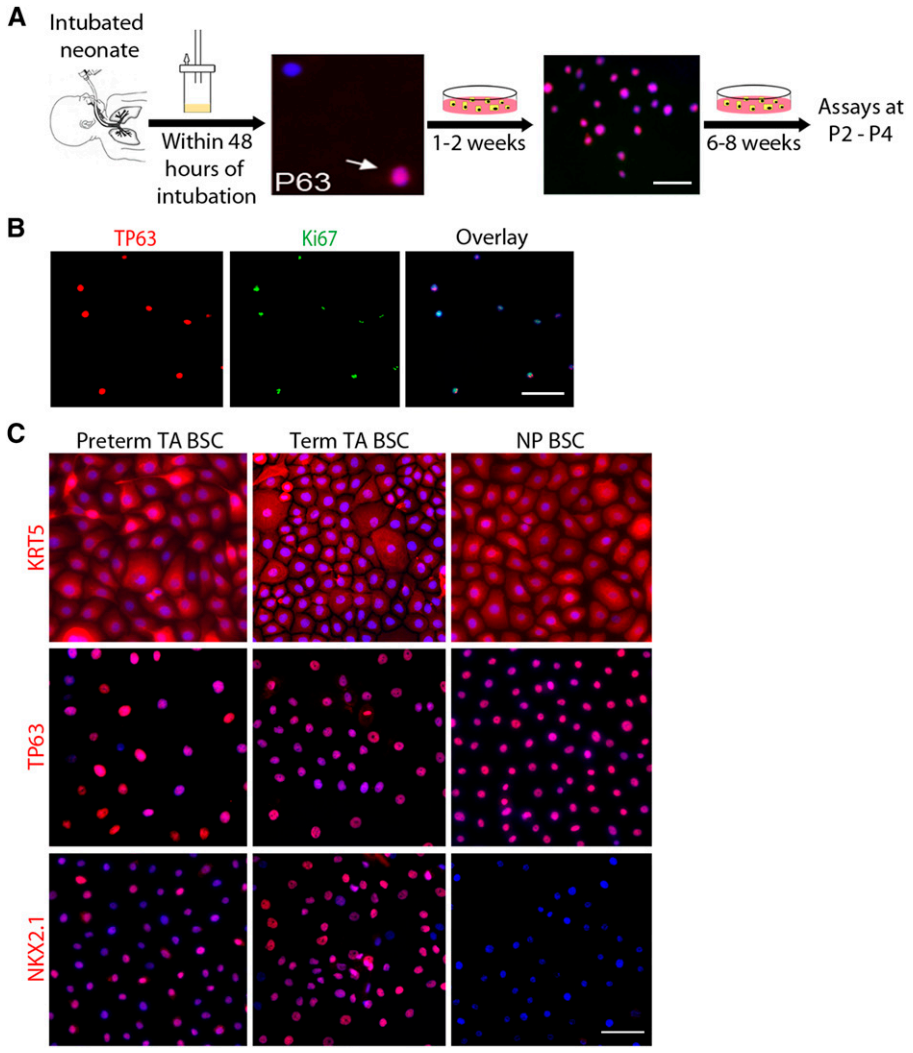

Figure 1. Tracheal aspirate (TA) basal stem cells (BSCs) are *bona fide* lower respiratory epithelial progenitor cells. (*A*) Schematic of the workflow. The images show TP63 staining of fresh neonatal TA sample (arrow) and the TA sample culture after 1–2 weeks. Cultures were expanded for 6–8 weeks and assayed at P2–P4. (*B*) Costaining for TP63 and Ki67 of BSC clones after 1–2 weeks in a culture of TA samples. (*C*) Representative images of KRT5, TP63, and NKX2.1 staining of confluent cultures of BSCs derived from TA and NP samples of term and preterm newborns. Scale bar, 25 μm. NP = nasopharyngeal; P2–P4 = passage 2–passage 4.

Methods

Human Samples

Patient enrollment, TA acquisition, and experiments were approved by the Institutional Review Board at Massachusetts General Hospital (IRB #2019P003296, PI: Lerou) and Boston Children's Hospital (IRB #2000P000372, PI: High). Demographic patient data are summarized in Table 1 (patients with CDH) and Table E1 in the online data supplement (control patients). Human fetal lung sections were obtained from a previously established tissue bank at the University of Manitoba (IRB #HS15293, PI: Keijzer) (18).

Nitrofen Rat Model of CDH

Animal work was approved by the Institutional Animal Care and Use Committee at Massachusetts General Hospital (IACUC #2022N000003, PI: Ai). Sprague-Dawley rat dams (Charles River Laboratory) at E9.5 were orally gavaged with nitrofen (100 mg in 1 ml olive oil) or olive oil (vehicle) (17). Dams received an intraperitoneal injection of dexamethasone (DXM) at E10.5 and E11.5 (0.25 mg/kg) and E12.5 (0.125 mg/kg) (30). Rat fetuses were harvested at E21.5.

Immunohistochemistry

Tracheas and lungs were fixed in 4% paraformaldehyde in phosphate-buffered saline and processed for paraffin embedding and sectioning before immunohistochemistry using standard staining procedures.

BSC Derivation, Expansion, and Differentiation Assays

Detailed protocols of TA BSC derivation, expansion, differentiation in ALI, and staining of ALI cultures for epithelial cell markers were recently published (28, 29). BSCs were treated with DXM (10 μM and 10 mM, Cat#D4902; Sigma Aldrich) on alternate days during 7-day cell expansion and for 7–21 days during ALI. For Poly (I:C) treatment (10 μM, Cat#tlrl-pic; Invivogen), BSCs were treated every 2 days during 7-day cell expansion followed by treatment at days 3, 5, 7, and 14 in ALI. For treatment with a specific nuclear factor kappa B (NF-kB) inhibitor JSH-23 (10 μM, Cat#S7351; Selleck Chemicals), ALI cultures were treated daily during the first week of differentiation. Bulk RNA sequencing and assay for transposase accessible chromatin with (ATAC) sequencing of BSCs were performed by ActiveMotif.inc.

Statistical Analysis and Data Availability

R-Studio and GraphPad Prism 6 were used for data analyses. Data in all graphs represent mean ± SEM from minimally three independent experiments. For comparisons between two or more conditions, statistical significance was analyzed using the Mann-Whitney *U* test, Student's *t* test, or Kruskal-Wallis test when appropriate. Statistical significance was considered if the *P* value was less than 0.05. All sequencing data can be accessed at the National Center for Biotechnology Information Gene Accession Omnibus via accession number GSE211790.

More details of materials and methods are provided in the online data supplement.

Results

BSCs Derived from TA Are *Bona Fide* Lower Respiratory Epithelial Progenitors

We collected TAs from newborns within the first 48 hours of intubation for BSC derivation to minimize the impact of

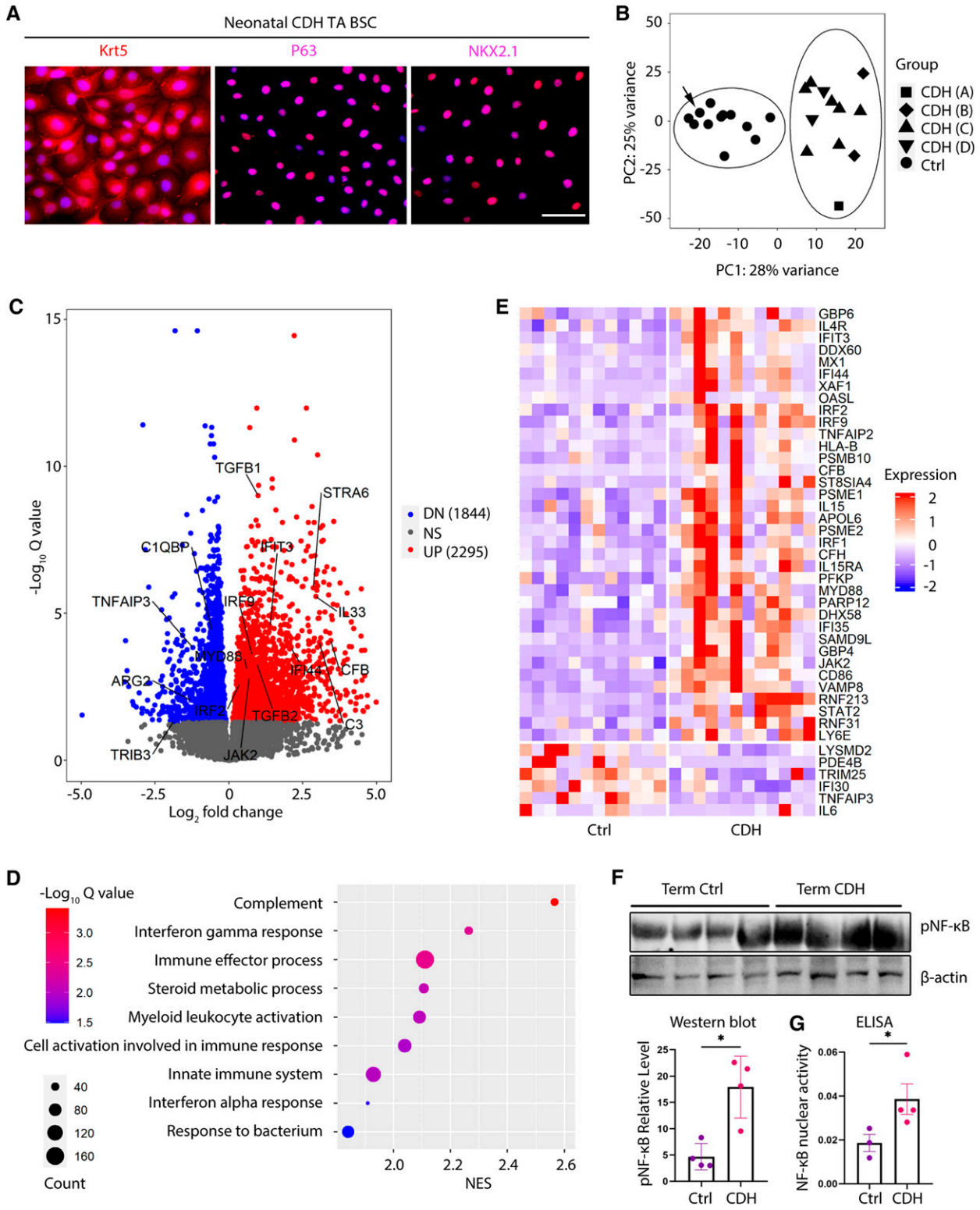

Figure 2. Congenital diaphragmatic hernia (CDH) basal stem cells (BSCs) have a disease-associated transcriptome and exhibit a proinflammatory signature. (*A*) Representative images of antibody staining for KRT5, TP63, and NKX2.1 in BSCs derived from TA of newborns with CDH. (*B*) Principal component analysis of bulk RNA sequencing datasets of BSC samples from CDH newborns ($n = 12$) and control, term ($n = 6$), and preterm ($n = 6$) newborns. Patients with CDH are labeled with A, B, C, and D according to their reported type of defect size during surgical repair. Arrow indicates one control case with prenatal oligohydramnios-associated lung hypoplasia. (*C*) Volcano plot highlighting differentially expressed genes between CDH and control BSCs with an adjusted $P < 0.05$. (*D*) Pathway analysis for bulk RNA sequencing results

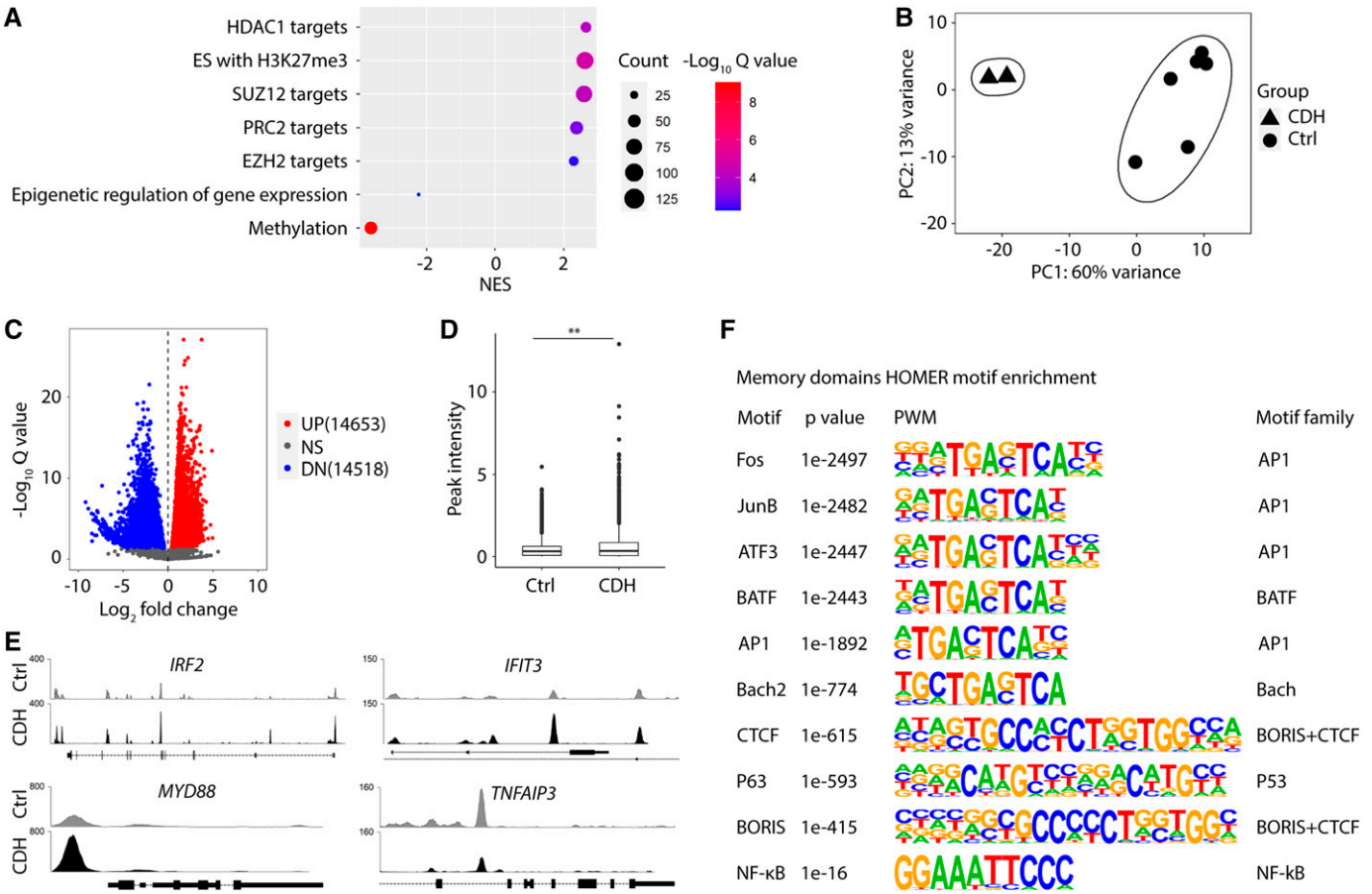

Figure 3. Basal stem cells (BSCs) from newborns with congenital diaphragmatic hernia (CDH) exhibit changes in chromatin accessibility. (*A*) Enrichment of target genes of epigenetic regulation among differentially expressed genes by bulk RNA sequencing between CDH and control BSCs. (*B*) Principal component analysis of assay for transposase accessible chromatin with sequencing datasets comparing CDH BSCs ($n = 2$) and control BSCs ($n = 6$). (*C*) Volcano plot highlighting significantly altered chromatin accessibility between CDH and control BSCs. (*D*) Summary of peak intensity within 1 kb surrounding the transcription start site of genes with at least one enriched peak between CDH and control BSCs. (*E*) Detailed examination of changes in peak signals within regulatory sequences of select genes. (*F*) HOMER motif analysis of chromatin accessibility. $^{**}P < 0.01$ by Student's *t* test. Ctrl = control; DN = downregulated; HOMER = hypergeometric optimization of motif enrichment; NS = not significant; NES = normalized enrichment score; NF-kB = nuclear factor kappa B; PC1 = principal component 1; PC2 = principal component 2; PWN = position weight matrix; UP = upregulated.

ventilation and postnatal clinical course on cellular phenotypes (Figure 1A). To establish that TA epithelial progenitors are BSCs from the lower respiratory tract, we showed that TAs contained rare TP63^{+} BSCs (Figure 1A). All TA BSCs proliferated to form clones after 1 week in culture (Figure 1B) and reached confluency within 3–4 weeks as passage 0 (P0). BSCs were collected at P2 for assays and cryopreservation in liquid nitrogen. Our pipeline from TA collection to BSC derivation has achieved a success rate of almost 100% per TA sample. In this study, bulk RNA sequencing and ATAC sequencing were performed at P2, and all other assays were conducted at P3–P4. Antibody staining and transcriptomic assays showed that all BSCs derived from TA of preterm and term newborns expressed basal cell markers, such as TP63 and KRT5, and NKX2.1, the lineage-specifying transcription factor of lower respiratory epithelial cells (Figures 1C and E1B) (21). In contrast, BSCs derived from nasopharyngeal swabs lacked NKX2.1 (Figure 1C) and exhibited significant differences in gene expression compared with TA BSCs (Figure E1) (31). These findings, together with our previous publications that TA BSCs can differentiate into multiple airway epithelial cell types (28, 29), indicate that TA BSCs are *bona fide* lower respiratory epithelial progenitors.

Figure 2. (*Continued*). of CDH and control BSCs. (*E*) Heatmap of interferon signaling pathway genes that are differentially expressed between CDH and control BSCs. (*F*) Representative Western blot for concentrations of Ser536 phosphorylation of the p65 subunit of nuclear factor kappa B (pNF-KB) in CDH ($n = 4$) and control ($n = 4$) BSCs. β-actin was a loading control. (*G*) Activity of nuclear NF-kB measured by ELISA in CDH BSCs ($n = 4$) and control BSCs ($n = 3$). $^{*}P < 0.05$ by Mann-Whitney *U* test. Scale bar, 25 μm. Ctrl = control; DN = downregulated; NS = not significant; pNF-KB = phosphorylated nuclear factor kappa B; TA = tracheal aspirate; UP = upregulated.

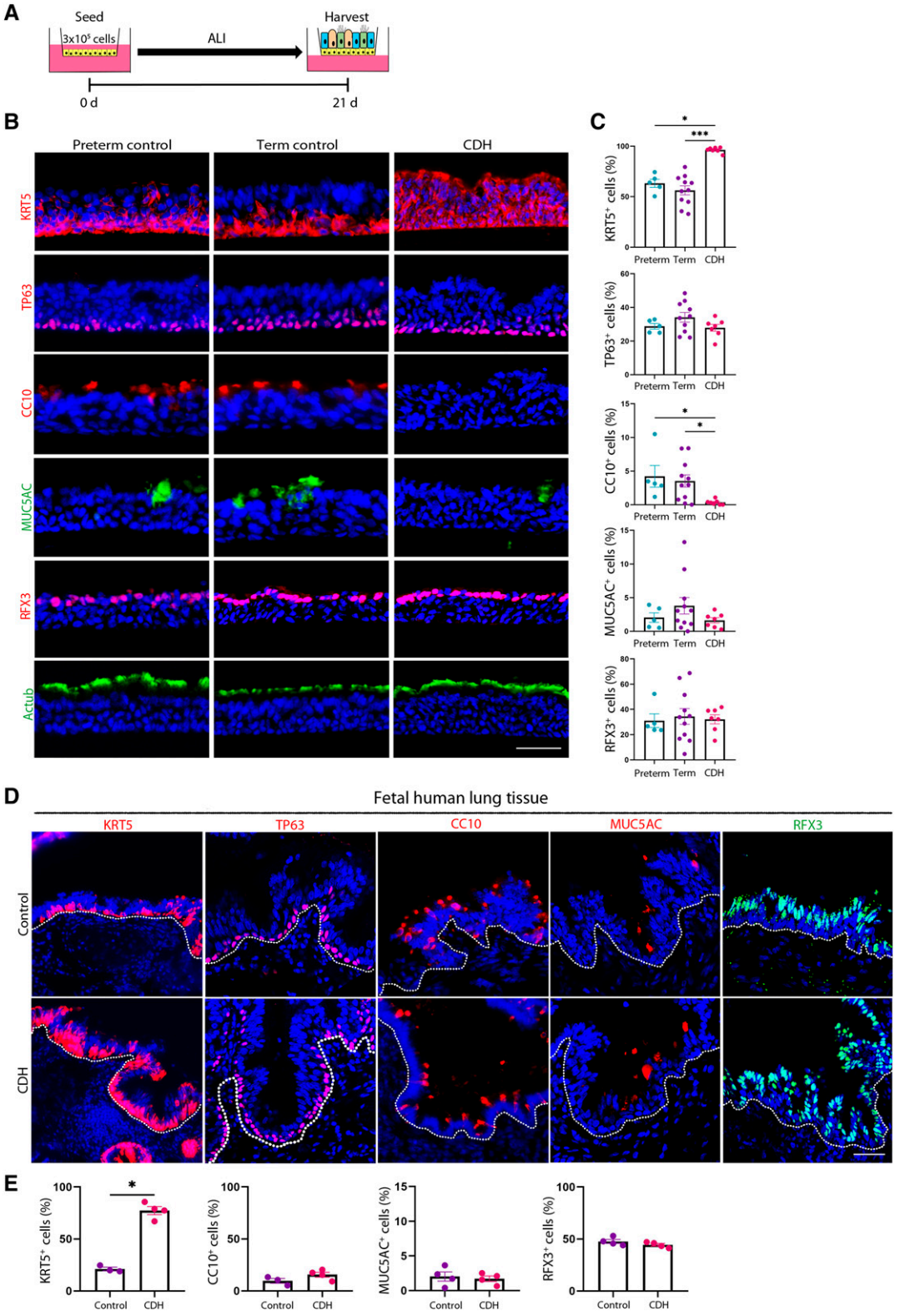

Figure 4. Congenital diaphragmatic hernia (CDH) basal stem cells (BSCs) have similar epithelial differentiation defects *in vitro* and *in vivo*. (*A*) Schematic of air–liquid interface (ALI) culture of preterm, term, and CDH BSCs for 21 days. (*B*) Representative fluorescence images of staining for markers of BSCs (KRT5 and TP63), club cells (CC10), goblet cells (MUC5AC), and ciliated cells (RFX3 and Actub) using cross-sections of fixed ALI cultures. Scale bar, 25 μM. (*C*) Quantification of the relative abundance of different epithelial cell types on the basis of the staining of ALI culture in triplicates. More than 6,000 nuclei in five 20× images were counted for each marker for each ALI culture. Each dot

Transcriptome Profiling Identifies a Proinflammatory Signature of CDH BSCs

We derived TA BSCs from 13 CDH newborns treated at Massachusetts General Hospital and Boston Children's Hospital. Most patients with CDH (9 out of 13) had left-sided hernias (Table 1). All four types of defect sizes (types A–D) (8) and various comorbidities were represented in this cohort (Table 1). Except for one preterm patient with CDH, all patients with CDH were born term at 36–40 weeks of gestation. Age-matched BSC control subjects were derived from control, term ($n = 11$), and preterm newborns ($n = 7$) who were intubated for reasons unrelated to congenital anomalies of the lung (Table E1). CDH BSCs and control BSCs displayed no difference in cell morphology and expression of basal cell markers and NKX2.1 (Figure 2A, compared with Figure 1C). We also did not observe significant changes between control and CDH BSCs in proliferation rate at an average of 28–32 hours per cell cycle.

To evaluate CDH-associated changes in gene expression, we performed bulk RNA sequencing of the first 12 derived CDH BSC lines and 12 randomly selected control BSC lines from six term and six preterm control newborns (Tables 1 and E1). One preterm control infant had oligohydramnios-related lung hypoplasia. Unsupervised principal component analysis determined no difference in transcriptomic profiles of preterm and term control BSCs (Figure E2). We thus combined these 12 control BSC lines as one control group for further analysis. CDH BSCs derived from patients with hernia sizes ranging from type A to D clustered together and separately from control subjects by principal component analysis (Figure 2B). These findings indicate that CDH deregulates the transcriptome of BSCs in a manner distinct from prematurity and independent of the hernia size.

Compared with control BSCs, CDH BSCs had 4,139 differentially expressed genes (DEGs, padj < 0.05), including 1,844 downregulated and 2,295 upregulated genes (Figure 2C). A disproportionally large number of DEGs in CDH were on chromosome 19 (Figure E3A). Many DEGs in CDH BSCs were related to inflammatory responses, including *MYD88, JAK2,* and interferon responsive genes (upregulated), and genes encoding for inhibitors of the NF-kB pathway (*TNFAIP3* and *TRIB3*) (downregulated) (Figures 2C, 2E, and E3B). Among epithelial differentiation signaling pathway genes, *STRA6* (a retinoic acid-responsive gene) (32), *TGFB1,* and *TGFB2* were significantly increased in CDH BSCs, whereas the expression of *WNT5A*, *WNT7B*, and *WNT9A* was similar between CDH BSCs and control BSCs (Figures 2C and E3B).

Gene set enrichment analysis found enrichment of DEGs in inflammatory processes, including the top two, complement and IFN-γ pathways (Figure 2D). A heatmap of DEGs involved in the IFN-γ pathway (33) showed an overall increase in expression in CDH BSCs compared with control subjects (Figure 2E). To test whether CDH BSCs had a hyperactive inflammatory response phenotype, we evaluated the status of NF-kB activation by quantifying phosphorylation of the p65 subunit. Western blot showed that CDH BSCs had a significant, approximately threefold increase in p65 phosphorylation compared with control BSCs (Figure 2F). We also detected significantly increased DNA binding activity of nuclear NF-kB by enzyme-linked immunosorbent assay in CDH BSCs ($n = 4$) compared with control BSCs ($n = 3$) (Figure 2G). Therefore, CDH BSCs display a proinflammatory signature.

Changes in Chromatin Accessibility in CDH BSCs Are Associated with a Proinflammatory Phenotype

CDH-associated changes in gene expression were maintained in cultured BSCs after derivation from TAs. Moreover, genes known to be epigenetically regulated were enriched in DEGs of CDH BSCs (Figure 3A). To test whether epigenetic mechanisms may underlie the proinflammatory signature of CDH BSCs, we compared chromatin accessibility profiles of CDH BSCs and control BSCs by ATAC sequencing (Figure 3B). Compared with control BSCs, CDH BSCs had 14,653 peaks with increased chromatin accessibility (upregulated domains) and 14,518 peaks with reduced accessibility (downregulated domains) (Figure 3C). We found a small but significant increase in signal density within the 1 kb region surrounding the transcription start sites of genes that had at least one differentially enriched peak (Figure 3D). *IRF2*, *IFIT3*, *MYD88*, *C3*, *CFB*, *TGFB1*, *TGFB2*, and *JAK2*, which were upregulated in CDH BSCs (Figures 2B, 2C, and 2E), had increased peak signals (Figures 3E and E3C). In contrast, downregulated genes in CDH BSCs, such as *TNFAIP3*, showed decreased peak signals (Figure 3E). In addition, within upregulated and downregulated domains in CDH BSCs, binding motifs for transcriptional factors with well-known roles in gene activation and inflammatory responses, such as AP1 family members, NF-kB, and TP63, were significantly enriched (Figure 3F). The binding motif for epigenetic insulators, CTCF and BORIS (34), was also enriched in upregulated and downregulated domains in CDH BSCs (Figure 3F), suggesting three-dimensional chromatin structural domains as a potential mechanism of gene regulation. Taken together, CDH BSCs register an aberrant chromatin accessibility profile that may facilitate transcriptional deregulation of genes involved in inflammatory responses.

CDH BSCs Exhibit Heterogenous Defects in Epithelial Differentiation

We tested whether CDH BSCs had changes in epithelial differentiation using Day 21 ALI cultures (Figure 4A). All 16 control BSC lines, including 5 preterm and 11 term lines, generated stratified airway epithelium with no difference in the abundance of residual BSCs ($KRT5^+$ cells, 63.3% ± 4.0% [preterm] vs. 56.3% ± 4.5% [term]; $P = 0.44$; $TP63^+$ cells, 28.8% ± 1.7% [preterm] vs. 34.1% ± 2.9% [term]; $P = 0.25$), $CC10^+$ club cells (4.2% ± 1.6% [preterm] vs. 3.5% ± 0.9% [term]; $P = 0.74$), $MUC5AC^+$ goblet cells (2.0% ± 0.7% [preterm] vs. 3.8 ± 1.2% [term]; $P = 0.66$), and $RFX3^+$

Figure 4. (*Continued*). represents one BSC line. (*D*) Representative fluorescence images of immunostaining for KRT5, TP63, CC10, MUC5AC, and RFX3 and in term, control ($n = 3$), and CDH ($n = 4$) human fetal lung sections. Scale bar, 50 μm. More than 2,000 nuclei in five images were counted per sample. (*E*) Quantification of the relative abundance of epithelial cells expressing individual markers on the basis of the staining of human fetal lung sections. Bar graphs show mean ± SEM. Statistical analyses were performed using the Kruskal-Wallis test for comparisons of multiple experimental groups and the Mann-Whitney *U* test for comparisons between two groups. Significance indicated as $^*P < 0.05$ and $^{***}P < 0.001$.

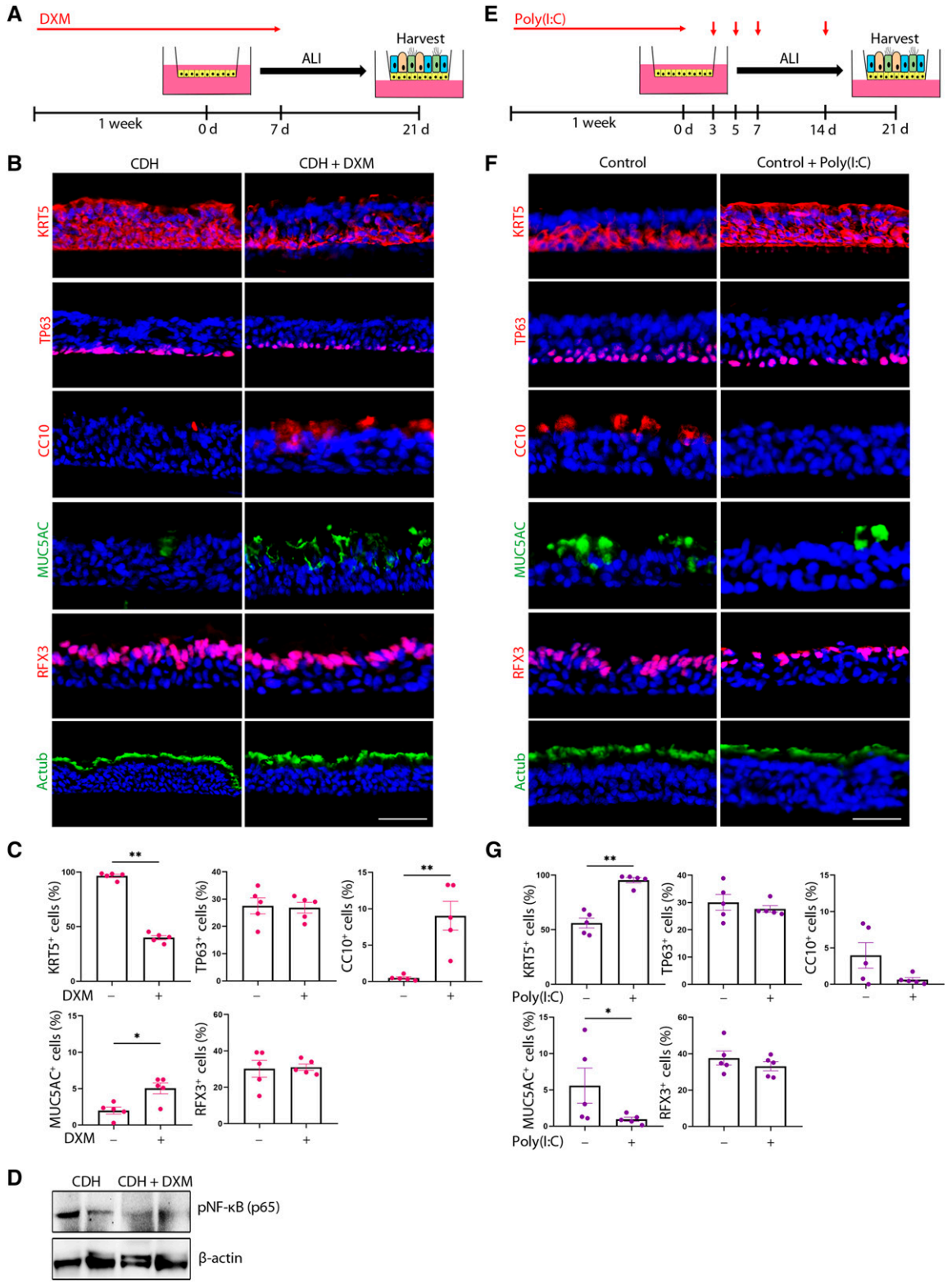

Figure 5. Dethamexasome (DXM) rescues differentiation defects of congenital diaphragmatic hernia (CDH) basal stem cells (BSCs) in air–liquid interface (ALI) cultures, whereas Poly(I:C) stimulation of control BSCs induces differentiation defects similar to those of CDH BSCs. (*A*) Schematic of the workflow. DXM (10 μM) was added during 1 week of cell expansion and the first week during ALI differentiation of CDH BSCs. (*B*) Representative fluorescence images of antibody staining for epithelial cell markers in Day 21 ALI cultures of CDH BSCs ($n = 5$ lines) with and without DXM treatment. Nuclei were stained by 4′,6-diamidino-2-phenylindole. (*C*) The relative abundance of each labeled cell type was quantified for each condition in triplicates. Each dot represents one CDH BSC line. (*D*) Representative Western blot for phosphorylated

ciliated cells (31.0 ± 5.4% [preterm] vs. 34.4% ± 6.2% [term]; $P = 0.91$) (Figures 4B and 4C). These results indicate that gestational age at birth has no effect on the differentiation potential of BSCs *in vitro*, which is consistent with similar transcriptomic profiles between preterm and term control BSCs (Figure 2B).

In contrast, 6 out of 13 CDH cell lines failed to differentiate in ALI after multiple attempts at varied cell seeding densities. The other seven CDH lines were able to differentiate; however, the generated airway epithelium was abnormal. KRT5 was retained in nearly 100% of cells (96.3% ± 1.0% [CDH]; $P < 0.05$), including cells already expressing differentiated epithelial markers. Moreover, club cell numbers were significantly reduced (0.34% ± 0.1% [CDH]; $P < 0.05$) compared with control ALI cultures (Figures 4B, 4C, and E4). CDH BSCs had no significant change in differentiation into ciliated cells and goblet cells (Figures 4B and 4C). Furthermore, the differentiation phenotypes of CDH BSCs were not caused by delayed differentiation, as they remained unchanged even after prolonged ALI culture for 35 days (Figure E5). Lastly, only 105 genes were differentially expressed between the seven CDH BSCs that were able to differentiate and six CDH BSCs that failed to differentiate (Figure E6), which precludes reliable pathway predictions for further testing. Taken together, CDH BSCs were defective in differentiation; however, their differentiation phenotypes are not identical despite a shared proinflammatory signature.

CDH BSCs Partially Reproduce the Epithelial Phenotype in Patients with CDH

To assess epithelial defects in patients with CDH, we examined lung sections from fetopsy samples of term, CDH ($n = 4$), and non-CDH control fetuses ($n = 3$) that were not treated (18). First, the control fetal airway epithelium *in vivo* contained differentiated epithelial cell types in relative abundance similar to that in control ALI cultures. Second, CDH lungs had more abundant $KRT5^+$ cells than control subjects (70.1% ± 5.1% vs. 30.4% ± 5.9%; $P < 0.01$) (Figures 4D and 4E), which is consistent with altered epithelial differentiation *in vitro* (Figures 4B and 4C). We did not observe changes in the abundance of $TP63^+$ basal cells, $RFX3^+$ ciliated cells, and $MUC5AC^+$ goblet cells in CDH airways compared with control subjects (Figures 4D and 4E). However, we found a significant number of ciliated cells marked by Actub that were also $KRT5^+$ in CDH airways, which resembles our observations in CDH ALI cultures (Figures E4C and E4D). We found no change in $CC10^+$ club cells in the intrapulmonary airway epithelium of CDH fetuses (Figures 4D and 4E). The discrepancy in club cell differentiation between *in vitro* and *in vivo* assays may be explained by a compensatory increase in club cell differentiation from other epithelial progenitors that coexist with BSCs in fetal human conducting airways (35).

The Proinflammatory Signature of CDH BSCs Underlies Abnormal Epithelial Differentiation

To test whether the proinflammatory signature of CDH BSCs may deregulate epithelial differentiation, we treated CDH BSCs with DXM, an antiinflammatory drug approved for induction of lung maturation in cases of preterm birth and tested effective in animal models of CDH (30, 36–38). We first tested whether DXM could restore epithelial differentiation in the subset of CDH BSCs that were able to differentiate (Figures 5A and E7). We showed that epithelial differentiation of CDH BSCs was normalized by minimally 2 weeks of DXM treatment (10 μM), including 1 week before ALI and during the first week in ALI (Figures 5A–5C and E7). This was documented by reduced $KRT5^+$ cells (96.3% ± 1.0% vs. 39.9% ± 1.9%; $P < 0.0001$) and rescued club cell differentiation ($CC10^+$, 0.34% ± 0.1% vs. 9.0% ± 2.0%; $P < 0.01$). Other cell types in ALI culture were unchanged by DXM treatment (Figures 5B and 5C). Accordingly, DXM treatment reduced the concentration of p65 phosphorylation in CDH BSCs by approximately 50% (Figure 5D). These beneficial effects of DXM were not improved by prolonged treatment or by using a higher concentration (10 mM) (Figure E7). DXM treatment had no effect on the differentiation of control BSCs (Figure E8). Furthermore, DXM treatment failed to rescue the other six CDH BSC lines that were incapable of differentiation in ALI. A specific NF-kB inhibitor, JSH-23 (10 μM), had similar rescue effects as DXM on CDH BSC differentiation without any effect on control BSCs (Figure E9). In addition, because the IL-6 and STAT3 pathway plays established roles in inflammation and BSC differentiation (39), we evaluated whether STAT3 activation may be involved in the differentiation phenotypes of CDH BSCs. We found no difference in baseline concentrations of phosphorylated, active STAT3 in control and CDH BSCs (Figure E10A). Correspondingly, the blockade of STAT3 activities had no effect on the differentiation of CDH BSCs (Figures E10B–E10D).

Poly(I:C), a mimic of double-stranded viral RNA, induces activation of the NF-kB and interferon pathways in multiple cell types, including airway epithelial cells (40, 41). Because CDH BSCs exhibited NF-kB hyperactivity and elevated concentrations of interferon response gene expression (Figures 2D–2F), we tested whether Poly(I:C) treatment of control BSCs mimicked the impact of CDH on epithelial differentiation. To do so, control BSCs ($n = 5$) were treated with 10 μM Poly(I:C) for 1 week before ALI and on Days 3, 5, 7, and 14 during ALI culture (Figure 5E). Poly(I:C)-treated cell lines responded with elevated NF-kB nuclear transcriptional activity (Figure E8D). Day 21 ALI cultures of Poly(I:C)-treated control BSCs showed an increase in $KRT5^+$ cells to almost 100% and a reduction in the number of club and goblet cells (Figures 5F and 5G), which is similar to CDH BSC differentiation (Figures 4B and 4C). In conclusion, the proinflammatory signature in CDH BSCs, manifested by hyperactive NF-kB and interferon pathways, is functionally linked to

Figure 5. (*Continued*). Ser536 in the p65 subunit (phosphorylated nuclear factor kappa B) in CDH BSCs with and without DXM treatment ($n = 2$) for 1 week during cell culture. β-actin was a loading control. (*E*) Schematic of the workflow. Poly(I:C) (10 μM) was added for the first week during ALI differentiation of control BSCs. (*F*) Representative fluorescence images of antibody staining for epithelial cell markers in Day 21 ALI cultures of control BSCs with and without Poly(I:C) treatment. (*G*) The relative abundance of each labeled cell type was quantified for each condition in triplicates. Each dot represents one control BSC line. ALI culture was performed in triplicates, and more than 6,000 cells were counted using stained sections of fixed ALI cultures for each BSC line. Bar graphs show mean ± SEM. $^*P < 0.05$ and $^{**}P < 0.01$ by Mann-Whitney *U* test. Scale bar, 25 μm.

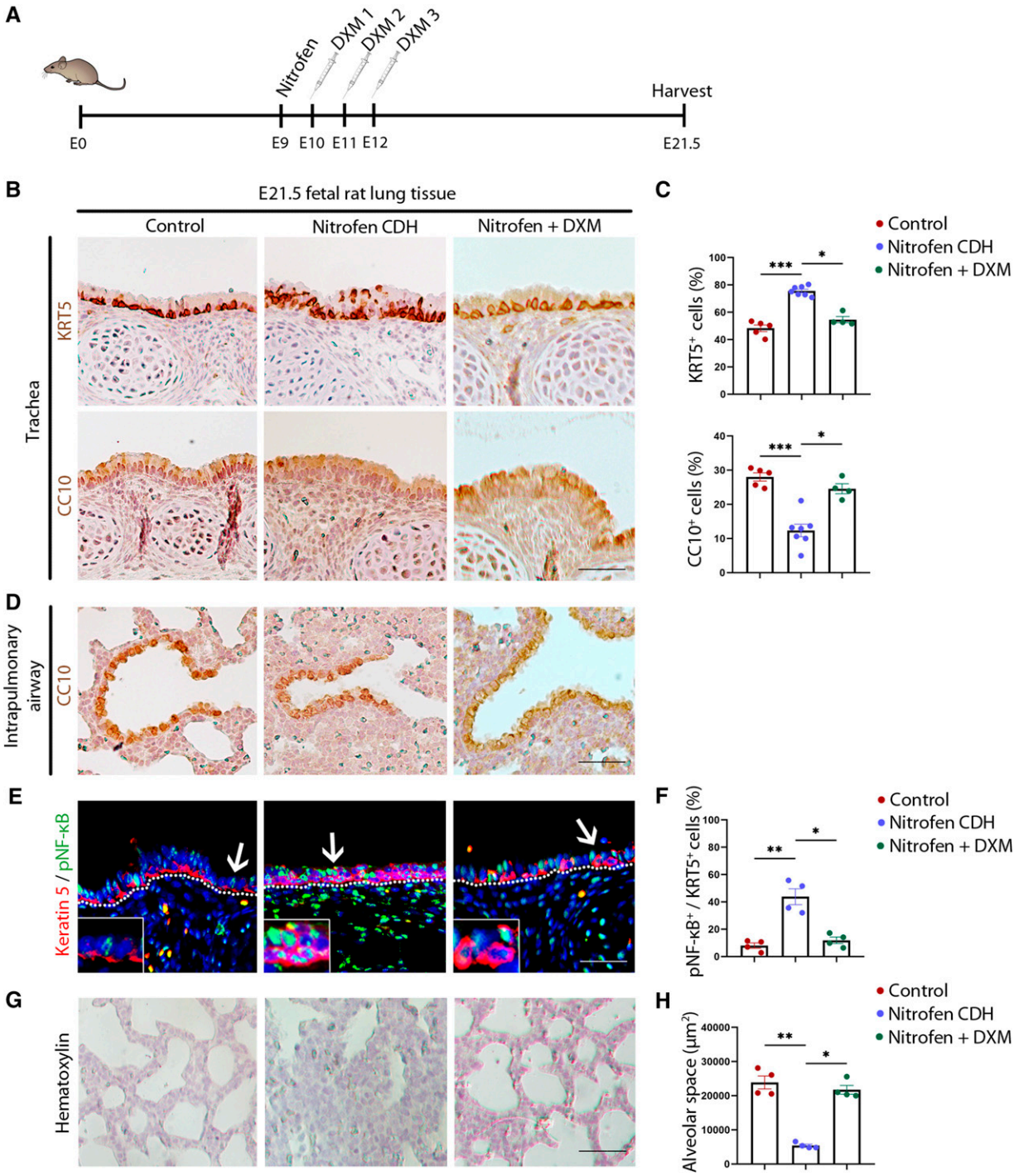

Figure 6. Dethamexasome (DXM) restores normal tracheal epithelium in rat fetuses of the nitrofen model of congenital diaphragmatic hernia (CDH). (*A*) Schematic of nitrofen (100 mg in olive oil) gavage at E9.5 and DXM administration (0.25 mg/kg at E10.5 and E11.5 and 0.125 mg/kg at E12.5). Control dams received olive oil. Fetuses were analyzed at E21.5. (*B*) Representative images of antibody staining for KRT5 and CC10 in fetal rat tracheas of control subjects ($n = 5$), nitrofen CDH ($n = 7$), and nitrofen with DXM ($n = 4$). (*C*) Quantification of the relative abundance of $KRT5^+$ and $CC10^+$ cells in the tracheal epithelium of each group. (*D*) Representative CC10 staining of intrapulmonary airway sections of each group. (*E*) Representative images of antibody costaining for KRT5 and phosphorylated nuclear factor kappa B (pNF-KB) in fetal rat tracheas of control subjects ($n = 4$), nitrofen CDH ($n = 4$), and nitrofen with DXM ($n = 4$). Arrow points to the epithelial area enlarged in the insert. (*F*) Quantification of the relative abundance of $pNF\text{-}KB^+KRT5^+$ double-positive cells among single-positive $KRT5^+$ cells in the tracheal epithelium of each group. (*G*) Representative hematoxylin staining of distal lung sections of each group. (*H*) Quantification of air space in the alveoli of each group. For quantification, more than three 20× images for each sample were quantified. Each dot represents one rat fetus, and fetuses from three dams were analyzed for each condition. Bar graphs show mean ± SEM. $^*P < 0.05$, $^{**}P < 0.01$, and $^{***}P < 0.001$ by Kruskal-Wallis test followed by a *post hoc* uncorrected Dunn's test. Scale bar, 20 μm.

abnormal epithelial differentiation in a subset of CDH BSCs.

Blockade of NF-kB Hyperactivity in the Rat CDH Model Normalizes Tracheal Epithelial Differentiation

To determine whether the beneficial effects of NF-kB inhibition on CDH BSC-based *in vitro* model could be reproduced *in vivo*, DXM (0.25 mg/kg) (30) was administrated to the nitrofen rat CDH model between E10.5 and E12.5 (Figure 6A) when BSCs are generated in the tracheal airway epithelium (24). Nitrofen exposure (E9.5) induced diaphragmatic hernia in 54% of fetuses (21 out of 39) and caused lung hypoplasia in 100% of fetuses (39 out of 39) at E21.5 in our study. The rat CDH tracheal epithelium has an increase in the number of $KRT5^+$ epithelial cells and a decrease in the number of $CC10^+$ club cells (Figures 6B and 6C). These changes resemble epithelial abnormalities in ALI cultures of CDH BSCs and human fetal CDH lungs (Figure 4). In contrast, club cells in intrapulmonary airways of nitrofen-exposed fetuses were unaffected (Figure 6D). Of note, club cells in rodent intrapulmonary airways can be generated from epithelial progenitors distinct from BSCs (21, 24, 42). These findings suggest that BSCs may be preferentially affected in the nitrofen model. Also consistent with elevated NF-kB signaling in CDH BSCs (Figures 2F and 2G), nitrofen-treated rat tracheal epithelium had elevated nuclear NF-kB in $KRT5^+$ cells (Figures 6E and 6F). After DXM administration, the occurrence of diaphragmatic hernia was seen in 33% of fetuses (9 out of 27). Importantly, the nitrofen-exposed tracheal epithelium was normalized, evidenced by KRT5 localization to the basal cell layer, recovered club cell differentiation, and reduced nuclear NF-kB in $KRT5^+$ cells to baseline (Figures 6B, 6C, 6E, and 6F). DXM also restored air space in the alveoli of nitrofen-exposed fetuses (Figures 6G and 6H), consistent with previous findings (30, 37, 38). Similar beneficial effects of *in vivo* JSH-23 administration (5 mg/kg) (43–45) on tracheal epithelial differentiation and NF-kB concentrations were also observed (Figure E11). Therefore, the blockade of hyperactive NF-kB normalizes lung phenotypes in the rat nitrofen model of CDH.

Discussion

In this study, we present a robust methodology of BSC derivation from TAs to model epithelial defects of CDH newborns *in vitro*. We provide evidence that CDH BSCs *in vitro* reproduce epithelial defects in human fetal CDH lungs and tracheas of the nitrofen rat model of CDH. This translational model enables the identification of a developmental defect of BSCs in CDH manifested by a proinflammatory signature that disrupts epithelial differentiation. Our approach of TA BSC derivation can be expanded to other neonatal lung diseases that affect the conducting airway for disease modeling and therapeutic testing *in vitro*. The proinflammatory signature in CDH BSCs is in accordance with a recent proteomic study that found elevated inflammatory responses in nitrofen CDH lungs (46). Specifically, elevated NF-kB in proximal epithelial cells during murine lung development can cause distal lung hypoplasia (47). Additional studies emphasize the crosstalk between inflammatory mediators and pathways involved in branching morphogenesis and epithelial differentiation (39, 47–51). By expanding on these findings, our results may inform the pathogenesis of lung defects in CDH.

We demonstrate that TAs are an alternative source of patient-specific lung cells to circumvent the technical difficulties of accessing fresh lung tissue in newborns. TA-derived BSCs also offer additional advantages, including time- and cost-effectiveness, compared with generating patient-specific human lung cells using induced pluripotent stem cell-based approaches (52). More importantly, by maintaining both the genetic and epigenetic landscapes, TA BSCs enable the characterization of patient-specific phenotypes with greater fidelity than induced pluripotent stem cell-based–derived lung progenitors that have undergone epigenetic reprogramming.

We acknowledge that our study using one type of epithelial progenitors harvested around birth is limited in reproducing complex interactions between multiple cell types during lung development. However, this concern is mitigated by similar epithelial phenotypes observed in our BSC culture system, CDH human fetal patient samples, and the nitrofen rat model of CDH. Future studies will investigate how abnormal BSC differentiation phenotypes relate to lung hypoplasia in patients with CDH.

Although previous studies suggested that CDH lungs may be developmentally premature (1, 2), we show that CDH BSCs display divergent transcriptome, chromatin accessibility, and differentiation when compared with preterm BSCs. Thus, CDH BSCs are not simply in a premature state. Furthermore, the size of the diaphragmatic hernia has no significant impact on the gene expression or differentiation capacity of CDH BSCs. These findings suggest the proinflammatory signature of CDH BSCs as an intrinsic mechanism of abnormal epithelial differentiation in CDH.

Recent reports show encouraging results for prenatal treatment of severe CDH cases using fetoscopic endoluminal tracheal occlusion (53). Novel therapeutics, such as amniotic fluid-derived extracellular vesicles, can promote prenatal lung maturation in CDH animal models (54). Here, our findings show the beneficial effects of antenatal NF-kB inhibitors on conducting airway epithelium, which is in line with improved lung phenotypes in the nitrofen rat model and surgical sheep model of CDH after steroid treatment (30, 37, 38). However, a small clinical trial assessing the effect of betamethasone during the last trimester of CDH pregnancies did not show improved outcomes (55). The limitations of this trial, however, include the small number of patients, and a single dosage and timing of treatment. Future studies could explore how such therapeutics can rescue CDH phenotypes in *in vitro* and large animal models before clinical testing in patients with CDH when applied alone or in combination with fetoscopic endoluminal tracheal occlusion (56). Lastly, correlating patient-specific *de novo* mutations with phenotypes of TA BSCs derived from the same patient cohorts is warranted to deepen our understanding of the pathogenesis of lung defects in CDH. ■

Author disclosures are available with the text of this article at www.atsjournals.org.

Acknowledgment: The authors thank Jennifer Lyu and Gheed Murtadi for coordinating TA collection from newborns with CDH.

References

1. Kitagawa M, Hislop A, Boyden EA, Reid L. Lung hypoplasia in congenital diaphragmatic hernia. A quantitative study of airway, artery, and alveolar development. *Br J Surg* 1971;58:342–346.
2. George DK, Cooney TP, Chiu BK, Thurlbeck WM. Hypoplasia and immaturity of the terminal lung unit (acinus) in congenital diaphragmatic hernia. *Am Rev Respir Dis* 1987;136:947–950.
3. Keijzer R, Puri P. Congenital diaphragmatic hernia. *Semin Pediatr Surg* 2010;19:180–185.
4. Wagner R, Montalva L, Zani A, Keijzer R. Basic and translational science advances in congenital diaphragmatic hernia. *Semin Perinatol* 2020;44: 151170.
5. Morsberger JL, Short HL, Baxter KJ, Travers C, Clifton MS, Durham MM, *et al.* Parent reported long-term quality of life outcomes in children after congenital diaphragmatic hernia repair. *J Pediatr Surg* 2019;54:645–650.
6. Dao DT, Patel N, Harting MT, Lally KP, Lally PA, Buchmiller TL. Early left ventricular dysfunction and severe pulmonary hypertension predict adverse outcomes in "low-risk" congenital diaphragmatic hernia. *Pediatr Crit Care Med* 2020;21:637–646.
7. Engels AC, Brady PD, Kammoun M, Finalet Ferreiro J, DeKoninck P, Endo M, *et al.* Pulmonary transcriptome analysis in the surgically induced rabbit model of diaphragmatic hernia treated with fetal tracheal occlusion. *Dis Model Mech* 2016;9:221–228.
8. Morini F, Valfrè L, Capolupo I, Lally KP, Lally PA, Bagolan P; Congenital Diaphragmatic Hernia Study Group. Congenital diaphragmatic hernia: defect size correlates with developmental defect. *J Pediatr Surg* 2013; 48:1177–1182.
9. Peiro JL, Oria M, Aydin E, Joshi R, Cabanas N, Schmidt R, *et al.* Proteomic profiling of tracheal fluid in an ovine model of congenital diaphragmatic hernia and fetal tracheal occlusion. *Am J Physiol Lung Cell Mol Physiol* 2018;315:L1028–L1041.
10. Donahoe PK, Longoni M, High FA. Polygenic causes of congenital diaphragmatic hernia produce common lung pathologies. *Am J Pathol* 2016;186:2532–2543.
11. Kardon G, Ackerman KG, McCulley DJ, Shen Y, Wynn J, Shang L, *et al.* Congenital diaphragmatic hernias: from genes to mechanisms to therapies. *Dis Model Mech* 2017;10:955–970.
12. McCulley DJ, Wienhold MD, Hines EA, Hacker TA, Rogers A, Pewowaruk RJ, *et al.* PBX transcription factors drive pulmonary vascular adaptation to birth. *J Clin Invest* 2018;128:655–667.
13. Ackerman KG, Wang J, Luo L, Fujiwara Y, Orkin SH, Beier DR. Gata4 is necessary for normal pulmonary lobar development. *Am J Respir Cell Mol Biol* 2007;36:391–397.
14. Domyan ET, Branchfield K, Gibson DA, Naiche LA, Lewandoski M, Tessier-Lavigne M, *et al.* Roundabout receptors are critical for foregut separation from the body wall. *Dev Cell* 2013;24:52–63.
15. Jay PY, Bielinska M, Erlich JM, Mannisto S, Pu WT, Heikinheimo M, *et al.* Impaired mesenchymal cell function in Gata4 mutant mice leads to diaphragmatic hernias and primary lung defects. *Dev Biol* 2007;301: 602–614.
16. Qiao L, Xu L, Yu L, Wynn J, Hernan R, Zhou X, *et al.* Rare and de novo variants in 827 congenital diaphragmatic hernia probands implicate LONP1 as candidate risk gene. *Am J Hum Genet* 2021;108: 1964–1980.
17. Kluth D, Kangah R, Reich P, Tenbrinck R, Tibboel D, Lambrecht W. Nitrofen-induced diaphragmatic hernias in rats: an animal model. *J Pediatr Surg* 1990;25:850–854.
18. Wagner R, Ayoub L, Kahnamoui S, Li H, Patel D, Liu D, *et al.* Establishment of a biobank for human lung tissues of congenital diaphragmatic hernia and congenital pulmonary airway malformation. *J Pediatr Surg* 2019;54:2439–2442.
19. Hogan BL, Barkauskas CE, Chapman HA, Epstein JA, Jain R, Hsia CC, *et al.* Repair and regeneration of the respiratory system: complexity, plasticity, and mechanisms of lung stem cell function. *Cell Stem Cell* 2014;15:123–138.
20. Rock JR, Onaitis MW, Rawlins EL, Lu Y, Clark CP, Xue Y, *et al.* Basal cells as stem cells of the mouse trachea and human airway epithelium. *Proc Natl Acad Sci USA* 2009;106:12771–12775.
21. Morrisey EE, Hogan BL. Preparing for the first breath: genetic and cellular mechanisms in lung development. *Dev Cell* 2010;18:8–23.
22. Montoro DT, Haber AL, Biton M, Vinarsky V, Lin B, Birket SE, *et al.* A revised airway epithelial hierarchy includes CFTR-expressing ionocytes. *Nature* 2018;560:319–324.
23. Zuo W, Zhang T, Wu DZ, Guan SP, Liew AA, Yamamoto Y, *et al.* p63(+)Krt5(+) distal airway stem cells are essential for lung regeneration. *Nature* 2015;517:616–620.
24. Yang Y, Riccio P, Schotsaert M, Mori M, Lu J, Lee DK, *et al.* Spatial-temporal lineage restrictions of embryonic $p63^{+}$ progenitors establish distinct stem cell pools in adult airways. *Dev Cell* 2018;44:752–761.e4.
25. Levardon H, Yonker LM, Hurley BP, Mou H. Expansion of airway basal cells and generation of polarized epithelium. *Bio Protoc* 2018;8:e2877.
26. Popova AP, Bozyk PD, Bentley JK, Linn MJ, Goldsmith AM, Schumacher RE, *et al.* Isolation of tracheal aspirate mesenchymal stromal cells predicts bronchopulmonary dysplasia. *Pediatrics* 2010;126: e1127–e1133.
27. Spadafora R, Lu J, Khetani RS, Zhang C, Iberg A, Li H, *et al.* Lung-resident mesenchymal stromal cells reveal transcriptional dynamics of lung development in preterm infants. *Am J Respir Crit Care Med* 2018; 198:961–964.
28. Amonkar GM, Wagner R, Bankoti K, Shui JE, Ai X, Lerou PH. Primary culture of tracheal aspirate-derived human airway basal stem cells. *STAR Protoc* 2022;3:101390.
29. Lu J, Zhu X, Shui JE, Xiong L, Gierahn T, Zhang C, *et al.* Rho/SMAD/mTOR triple inhibition enables long-term expansion of human neonatal tracheal aspirate-derived airway basal cell-like cells. *Pediatr Res* 2021; 89:502–509.
30. Losty PD, Pacheco BA, Manganaro TF, Donahoe PK, Jones RC, Schnitzer JJ. Prenatal hormonal therapy improves pulmonary morphology in rats with congenital diaphragmatic hernia. *J Surg Res* 1996;65:42–52.
31. Shui JE, Wang W, Liu H, Stepanova A, Liao G, Qian J, *et al.* Prematurity alters the progenitor cell program of the upper respiratory tract of neonates. *Sci Rep* 2021;11:10799.
32. Pasutto F, Sticht H, Hammersen G, Gillessen-Kaesbach G, Fitzpatrick DR, Nürnberg G, *et al.* Mutations in STRA6 cause a broad spectrum of malformations including anophthalmia, congenital heart defects, diaphragmatic hernia, alveolar capillary dysplasia, lung hypoplasia, and mental retardation. *Am J Hum Genet* 2007;80: 550–560.
33. Liberzon A, Birger C, Thorvaldsdóttir H, Ghandi M, Mesirov JP, Tamayo P. The molecular signatures database (MSigDB) hallmark gene set collection. *Cell Syst* 2015;1:417–425.
34. Marshall AD, Bailey CG, Rasko JE. CTCF and BORIS in genome regulation and cancer. *Curr Opin Genet Dev* 2014;24:8–15.
35. Nikolić MZ, Caritg O, Jeng Q, Johnson JA, Sun D, Howell KJ, *et al.* Human embryonic lung epithelial tips are multipotent progenitors that can be expanded in vitro as long-term self-renewing organoids. *eLife* 2017;6:e26575.
36. Grier DG, Halliday HL. Effects of glucocorticoids on fetal and neonatal lung development. *Treat Respir Med* 2004;3:295–306.
37. Burgos CM, Pearson EG, Davey M, Riley J, Jia H, Laje P, *et al.* Improved pulmonary function in the nitrofen model of congenital diaphragmatic hernia following prenatal maternal dexamethasone and/or sildenafil. *Pediatr Res* 2016;80:577–585.
38. Hedrick HL, Kaban JM, Pacheco BA, Losty PD, Doody DP, Ryan DP, *et al.* Prenatal glucocorticoids improve pulmonary morphometrics in fetal sheep with congenital diaphragmatic hernia. *J Pediatr Surg* 1997; 32:217–221. [Discussion, pp. 221–222.]
39. Tadokoro T, Wang Y, Barak LS, Bai Y, Randell SH, Hogan BL. IL-6/STAT3 promotes regeneration of airway ciliated cells from basal stem cells. *Proc Natl Acad Sci USA* 2014;111:E3641–E3649.
40. Dauletbaev N, Cammisano M, Herscovitch K, Lands LC. Stimulation of the RIG-I/MAVS pathway by polyinosinic:polycytidylic acid upregulates IFN-β in airway epithelial cells with minimal costimulation of IL-8. *J Immunol* 2015;195:2829–2841.
41. Ramezanpour M, Bolt H, Psaltis AJ, Wormald PJ, Vreugde S. Primary human nasal epithelial cells: a source of poly (I:C) LMW-induced IL-6 production. *Sci Rep* 2018;8:11325.
42. Rawlins EL, Okubo T, Xue Y, Brass DM, Auten RL, Hasegawa H, *et al.* The role of Scgb1a1+ Clara cells in the long-term maintenance and repair of lung airway, but not alveolar, epithelium. *Cell Stem Cell* 2009; 4:525–534.

43. Homme RP, Sandhu HS, George AK, Tyagi SC, Singh M. Sustained inhibition of NF-κB activity mitigates retinal vasculopathy in diabetes. *Am J Pathol* 2021;191:947–964.
44. Tong J, Hu C, Wu Y, Liu Q, Sun D. Radiation-induced NF-κB activation is involved in cochlear damage in mice via promotion of a local inflammatory response. *J Radiat Res (Tokyo)* 2022;64:63–72.
45. Kumar A, Negi G, Sharma SS. JSH-23 targets nuclear factor-kappa B and reverses various deficits in experimental diabetic neuropathy: effect on neuroinflammation and antioxidant defence. *Diabetes Obes Metab* 2011;13:750–758.
46. Wagner R, Lieckfeldt P, Piyadasa H, Markel M, Riedel J, Stefanovici C, *et al.* Proteomic profiling of hypoplastic lungs suggests an underlying inflammatory response in the pathogenesis of abnormal lung development in congenital diaphragmatic hernia. *Ann Surg* [online ahead of print] 3 Aug 2022; DOI: 10.1097/SLA.0000000000005656.
47. Benjamin JT, van der Meer R, Im AM, Plosa EJ, Zaynagetdinov R, Burman A, *et al.* Epithelial-derived inflammation disrupts elastin assembly and alters saccular stage lung development. *Am J Pathol* 2016;186:1786–1800.
48. Benjamin JT, Carver BJ, Plosa EJ, Yamamoto Y, Miller JD, Liu JH, *et al.* NF-kappaB activation limits airway branching through inhibition of Sp1-mediated fibroblast growth factor-10 expression. *J Immunol* 2010; 185:4896–4903.
49. Katsura H, Kobayashi Y, Tata PR, Hogan BLM. IL-1 and TNFα contribute to the inflammatory niche to enhance alveolar regeneration. *Stem Cell Reports* 2019;12:657–666.
50. LaCanna R, Liccardo D, Zhang P, Tragesser L, Wang Y, Cao T, *et al.* Yap/Taz regulate alveolar regeneration and resolution of lung inflammation. *J Clin Invest* 2019;129:2107–2122.
51. Strunz M, Simon LM, Ansari M, Kathiriya JJ, Angelidis I, Mayr CH, *et al.* Alveolar regeneration through a Krt8+ transitional stem cell state that persists in human lung fibrosis. *Nat Commun* 2020;11:3559.
52. Hawkins FJ, Suzuki S, Beermann ML, Barillà C, Wang R, Villacorta-Martin C, *et al.* Derivation of airway basal stem cells from human pluripotent stem cells. *Cell Stem Cell* 2021;28: 79–95.e8.
53. Deprest JA, Nicolaides KH, Benachi A, Gratacos E, Ryan G, Persico N, *et al.*; TOTAL Trial for Severe Hypoplasia Investigators. Randomized trial of fetal surgery for severe left diaphragmatic hernia. *N Engl J Med* 2021;385:107–118.
54. Antounians L, Catania VD, Montalva L, Liu BD, Hou H, Chan C, *et al.* Fetal lung underdevelopment is rescued by administration of amniotic fluid stem cell extracellular vesicles in rodents. *Sci Transl Med* 2021; 13:eaax5941.
55. Lally KP, Bagolan P, Hosie S, Lally PA, Stewart M, Cotten CM, *et al.*; Congenital Diaphragmatic Hernia Study Group. Corticosteroids for fetuses with congenital diaphragmatic hernia: can we show benefit? *J Pediatr Surg* 2006;41:668–674. [Discussion, pp. 668–674.]
56. Serapiglia V, Stephens CA, Joshi R, Aydin E, Oria M, Marotta M, *et al.* Fetal tracheal occlusion increases lung basal cells *via* increased Yap signaling. *Front Pediatr* 2022;9:780166.